Thellier paleointensity theory and experiments for multidomain grains

Song Xu[1] and David J. Dunlop

Geophysics, Physics Department, University of Toronto, Toronto, Ontario, Canada

Received 17 February 2004; revised 16 April 2004; accepted 3 May 2004; published 3 July 2004.

[1] We extend theories of thermoremanent magnetization (TRM) and partial TRM (pTRM) in multidomain (MD) grains to model thermal demagnetization and pTRM acquisition steps in Thellier paleointensity determination. Because of the interleaving of zero-field and in-field heating-cooling steps to increasing temperatures the initial state for any step is complex, and theoretical modeling is more intricate than for pTRM production or thermal demagnetization separately. At low to moderate temperature T, TRM lost exceeds pTRM regained, causing convex down Arai plots sagging below the ideal single-domain (SD) line. At moderate to high T, pTRM acquisition outweighs TRM loss. As T approaches T_{Curie}, pTRM gain exactly equals TRM loss, and the Arai plot becomes ideal. When pTRMs are produced perpendicular to the original TRM and measured directly rather than by differencing field-on and field-off results, there is less deviation from ideality at low to moderate T. Our theory agrees semiquantitatively with results for parallel and perpendicular pTRMs for large MD magnetites (135 μm). Smaller MD magnetites (6 and 20 μm) have less curved Arai plots, and the smallest magnetites (0.6 and 1 μm) have almost linear plots. Positive pTRM checks demonstrate that curved Arai plots of MD grains are reproducible, unlike curved plots for rocks that alter physicochemically in the Thellier experiment, while negative pTRM tail checks indicate undemagnetized pTRM residuals. Low-temperature demagnetization improves linearity only slightly. Practical applications of this work include using the predicted threshold T below which no net pTRM is produced in a parallel Thellier experiment to screen data used for paleointensity fits. Straight line fits through low- and medium-T points in Arai plots of MD (135 μm) grains overestimated the paleofield by as much as 100% and for small pseudo-single-domain (PSD) (0.6 and 1 μm) grains overestimated by about 25%. However, by using linear segments of medium- to high-T data with f values $\geq$0.5 it may be possible to obtain reasonable paleointensity estimates even for larger PSD (6 and 20 μm) and MD grains. Middle- to high-T fits for 0.6 μm grains gave paleointensities within 4% of the correct value, utilizing essentially the entire data set ($f > 0.9$). Perpendicular data always gave superior linear fits. Orienting samples with their natural remanent magnetizations perpendicular to the laboratory field is therefore recommended for rocks containing PSD and MD grains. However, double heatings are preferable to single heatings because they allow pTRM tail checks to be carried out. *INDEX TERMS:* 1521 Geomagnetism and Paleomagnetism: Paleointensity; 1540 Geomagnetism and Paleomagnetism: Rock and mineral magnetism; 1503 Geomagnetism and Paleomagnetism: Archeomagnetism; 1594 Geomagnetism and Paleomagnetism: Instruments and techniques; *KEYWORDS:* paleointensity determination, Thellier method, multidomain grains

Citation: Xu, S., and D. J. Dunlop (2004), Thellier paleointensity theory and experiments for multidomain grains, *J. Geophys. Res.*, *109*, B07103, doi:10.1029/2004JB003024.

1. Introduction

[2] Both the intensity and the direction of the ancient geomagnetic field are recorded by natural remanent magnetization (NRM) in rocks and sediments. Among magnetizing processes in nature, only thermoremanent magnetization (TRM) can be reproduced in the laboratory and used to determine absolute paleointensity. The *Thellier and Thellier* [1959] paleointensity method consists of pairs of heating-cooling steps to increasing temperatures T. As modified by *Coe* [1967], the first heating-cooling is in zero field and thermally demagnetizes a fraction of the NRM, which must be a TRM for the method to work. The second heating-cooling is in a laboratory field $\mathbf{H_L}$ and imparts a partial TRM (pTRM). Magnetic carriers of single-domain (SD) size have TRM unblocking temperatures T_{UB} that match their pTRM blocking temperatures T_B, so that the

[1]Now at JDL Digital Systems, Seattle, Washington, USA.

0148-0227/04/2004JB003024$09.00

pTRM gained in the second step will exactly replace the fraction of TRM lost in the first step, restoring the NRM to its initial value (assuming $\mathbf{H_L} = \mathbf{H_A}$, the ancient field).

[3] There are several advantages to the stepwise nature of the Thellier experiment. One has replicate estimates of $\mathbf{H_A}$, and by plotting results on a graph of NRM remaining versus pTRM gained for each T (an Arai diagram [*Nagata et al.*, 1963]), the data can be analyzed by least squares fitting. The ideal SD Arai plot (if $\mathbf{H_L} = \mathbf{H_A}$) is a straight line of slope -1. If the NRM has been modified, by secondary processes in nature or during laboratory heating, this is usually detectable on the Arai plot. Typical nonideal plots are due to thermoviscous remagnetization in geologically recent times, which affects low T_B/T_{UB} fractions, and laboratory chemical remanent magnetization (CRM), which affects high T_B/T_{UB} fractions. Fractions with intermediate T_B/T_{UB} may still be usable.

[4] The commonest magnetic mineral in continental rocks is magnetite. Only a minute fraction of naturally occurring magnetite is smaller than the critical SD size of 0.07–0.08 μm [*Enkin and Williams*, 1994; *Newell and Merrill*, 1999]. It has been known since the work of *Levi* [1977] that larger magnetites, of pseudo-single-domain (PSD) and multidomain (MD) size, have curved (convex down) Arai plots in which only the first and last data points fit the ideal line, but as *Shcherbakov and Shcherbakova* [2001] remark, "The question of why such plots occur remains mostly unsolved."

[5] The purpose of the present paper is to extend existing MD theories of TRM and pTRM [*Néel*, 1955; *Dunlop and Xu*, 1994; *Xu and Dunlop*, 1994] to analyze the sequence of field-off and field-on steps in the Thellier experiment and to test the theory experimentally using MD and PSD magnetites with mean grain sizes from 0.6 μm to 135 μm. Our theory is based on the reequilibration of domain walls by self-demagnetizing fields with changing T. It does not account for all features of multidomain TRM [*Shcherbakov et al.*, 1993; *McClelland et al.*, 1996; *Shcherbakova et al.*, 2000; *Shcherbakov and Shcherbakova*, 2001; *Shcherbakov et al.*, 2001], but it does give a good description of the stepwise thermal demagnetization and pTRM acquisition process in the Thellier experiment. It is physically based, not phenomenological like the model of *Fabian* [2000, 2001], and it has predictive power. We believe it accurately describes aspects of MD behavior controlled by domain wall motion for a fixed population of walls (no domain nucleation or annihilation in the T range covered by the Thellier experiment).

2. Theory for a Single Microcoercivity

[6] Following *Néel* [1955], we consider a planar domain wall of area A displaced a distance x from the central demagnetized position in a grain of width $2a$ and spontaneous magnetization M_s. The magnetization $M = (x/a)\, M_s$ is determined by minimizing the sum E of the magnetostatic energy $E_H = -2\mu_o A M_s H_o x$ due to the external applied field H_o, the wall energy E_w which changes with x because of varying pinning by lattice defects like dislocations, and the demagnetizing energy $E_d = \mu_o N A M_s^2 x^2/a$ (N is demagnetizing factor). Setting $dE/dx = 0$, one obtains

$$dE_w/dx = 2\mu_o A M_s (H_o - NM) = 2\mu_o A M_s H_i, \qquad (1)$$

where the average internal field is

$$H_i = H_o - NM. \qquad (2)$$

One can proceed to a direct solution, minimizing E and finding M numerically [*Schmidt*, 1973], but there are some advantages to solving equations (1) and (2) as simultaneous parametric equations in H_i, as *Néel* [1955] did.

[7] One advantage is that microcoercivity h_c is defined in terms of the internal field, as the critical value of H_i required to unpin a wall trapped by crystal defects [e.g., *Xu and Merrill*, 1989]. From equation (1) it follows that $h_c = (2\mu_o A M_s)^{-1} (dE_w/dx)_{max}$ within the local potential well where the wall is trapped. However, because of self-demagnetization, the microcoercivity measured in terms of the external field H_o is not symmetric, being $> h_c$ if the wall is being pushed away from a demagnetized state but $< h_c$ if the wall moves toward a demagnetized state [*Dunlop and Xu*, 1994; *Dunlop and Özdemir*, 1997].

[8] A second advantage is that the treatment by equations (1) and (2) separately has a simple and instructive graphical representation (Figure 1). If the barriers to wall motion are identical and regularly spaced, equation (1) gives a rectangular $M(H_i)$ loop with a single value of h_c equal to the measured bulk coercive force H_c. Equation (2) leads to T-independent lines of slope $-1/N$, with intercepts H_o in TRM/pTRM acquisition, or zero in thermal demagnetization. Intersections between these demagnetizing lines and the internal field loop give $M(H_o)$. Alternatively, "shearing" the $M(H_i)$ loop until the demagnetizing lines become vertical yields the $M(H_o)$ loop [*Néel*, 1955].

[9] The basic reason for TRM blocking is apparent by comparing the loop intersections at various T (Figure 1). Experimentally H_c varies with T as a power of M_s:

$$H_c = H_c(T_o)\, [M_s(T)/M_s(T_o)]^n = H_{co}\, \beta^n(T), \qquad (3)$$

where T_o is room temperature. Therefore the vertical and horizontal arms of the $M(H_i)$ loop expand at different rates during cooling from the Curie temperature T_C. At first, the intersections with the demagnetizing line for fixed field H_o descend the vertical arm of the loop. The decreasing values of M/M_s that result show that the demagnetizing field $H_d(T)(\sim M_s(T))$ is pushing walls back toward a demagnetized state against the resistance of pinning, as expressed by $H_c(T)$. However, past a certain point the intersections begin to ascend the vertical loop. These are virtual intersections because it is physically impossible for $M/M_s = x/a$ to increase unless the magnetizing field H_o increases. Instead, the wall remains trapped in a local E_w well. This process is referred to as field blocking, and the temperature at which it occurs is the blocking temperature T_B [*Néel*, 1955].

[10] The partial TRM process is more complex than blocking of total TRM because if $H_o \to 0$ not too far below T_B, H_d may drive the wall back. This process is called wall reequilibration. In thermal demagnetization, reequilibration is dominant and often begins immediately above T_o and continues practically to T_C. A single blocking temperature T_B leads to a spectrum of unblocking temperatures T_{UB} both $< T_B$ and $> T_B$, sometimes referred to as low-T and high-T tails in the spectrum $f(T_{UB})$ [*Dunlop and Özdemir*, 2001].

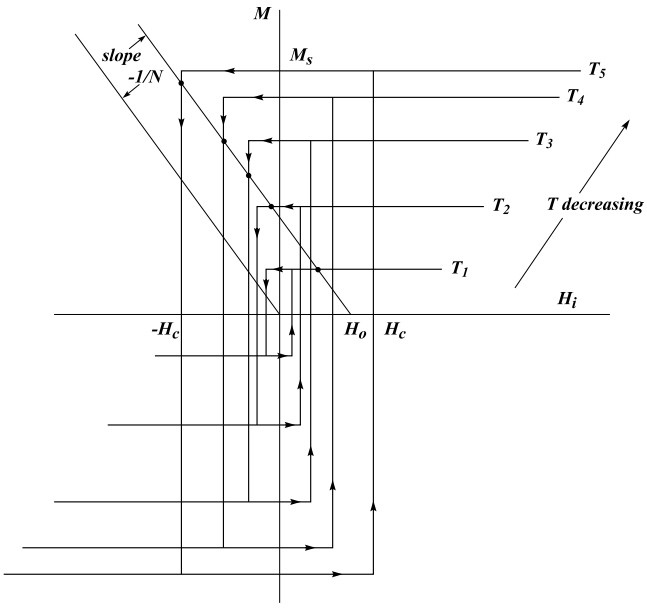

Figure 1. Graphical procedure for obtaining $M(H_o)$ from intersections (dots) between internal field hysteresis loops, $M(H_i, T)$ (rectangular), and inclined T-independent demagnetizing lines, $M(H_i, H_o)$ (equation (2)), of slope $-1/N$ and intercept H_o in partial thermoremanent magnetization (pTRM) acquisition or zero in thermal demagnetization.

[11] The mathematical details of pTRM blocking and thermal demagnetization are covered thoroughly by *Dunlop and Xu* [1994]. The novelty comes in the stepwise interweaving of the two processes in the Thellier experiment. The example in Figure 2 has model parameters $H_{co} = H_c(T_o) = 2$ mT, $H_o = 0.5$ mT, and $n = 2$, which were used in many of the examples given by *Dunlop and Xu* [1994] because they lead to a relatively low T_B of 495°C. Smaller H_o lead to high blocking temperatures and a compressed range of Thellier steps; for example, $H_o = 50$ μT gives $T_B = 570$°C, just below $T_C = 580$°C.

[12] Figure 2 models a Thellier experiment; 2 and 3, 4 and 5, etc., are twin heating-cooling steps to increasing T, the first in zero field (thermal demagnetization) and the second in H_o (pTRM production). We begin at $T = 530$°C because all lower steps result in thermal demagnetization of the "NRM" (which is a total TRM, produced in step 1) but no pTRM acquisition: The walls reequilibrate when $H_o \rightarrow 0$ at T_o. Starting with TRM production, the intersection point during cooling follows the "TRM blocking master curve" (the locus defined by the intersections in Figure 1) down to its minimum at $T_B = 495$°C (point 1). The TRM blocked is about 1% of M_s ($r = M/M_s = x/a = 0.01$). Because Figure 2 is plotted in terms of $r = M/M_s$ rather than M, the demagnetizing lines $H_i = H_o - NM = H_o - NrM_s(T)$ now have slopes that vary with T. Thus when $H_o \rightarrow 0$ at T_o, the new intersection 1 (left-hand axis) is with a line of lower slope, $H_i = -Nr_oM_{so}$.

[13] Stepwise thermal demagnetization, for our choice of parameters, results in M decreasing in proportion to $\beta^{n-1}(T) = \beta(T)$ for $n = 2$ [*Dunlop and Xu*, 1994, section 4.2]. The thermal demagnetization master curve (Figure 2) is constructed so that its intersections with the lines $H_i = -NrM_s(T)$ follow this relation. At $T = 530$°C this intersection is 2; the normalized NRM has decreased to $r = 0.4\%$ by this heating. This same value of r is preserved as r_o after cooling to T_o, where measurements are made (point 2′). With this as an initial state we do a second heating to $T = 530$°C and cooling to T_o, this time in $H_o = 0.5$ mT. At 530°C, H_c has decreased from 2 to about 0.32 mT (ascending loop shown dashed). The intersection point 3v with the line $H_i = H_o - NrM_s$ (530°C) is virtual: It predicts a magnetization less than the surviving NRM. Thus r and r_o (3 and 3′) remain at the previous level 2, 2′. Physically, we are still in the reequilibration regime.

[14] The initial state for the thermal demagnetization step to 540°C is 2′. Heating to 530°C gives intersection 4, and heating to 540°C gives 4′, which is retained as r_o at T_o (point 4″). The second, in-field heating to 540°C starts from 4″ and proceeds to 5, the intersection between the ascending $M - H_i$ loop at 540°C and the line $H_i = H_o - NrM_s$ (540°C). This value of r is preserved by field cooling to T_o, giving an r_o of about 0.37% (point 5′). For the first time, there is a net pTRM produced, amounting to about 0.02% (the difference between 5′ and 4″, the results of the field-on and field-off steps).

[15] The 550°C, 558°C, and 563°C double-heating steps proceed in the same fashion. Starting from initial state 5′, thermal demagnetization proceeds to 6 (at 540°C), 6′ (at 550°C), and 6″ (at T_o). This is the NRM remaining after 550°C. From initial state 6″ we carry out the field-on heating to 550°C, giving intersection point 7 with the ascending loop, and field cooling to T_o, giving 7′. The change in NRM between 540° and 550°C (Δr_o between 4″ and 6″) is small, about 0.06%. The calculated pTRM gain, Δr_o between 7′ and 6″, is considerably larger than the NRM loss, amounting to about 0.24% or ¼ of the total TRM. This pattern continues for the 558°C (7′, 8, 8′, 8″ plus 8″, 9, and 9′) and 563°C (9′, 10, 10′, 10″ plus 10″, 11, and 11′) steps, with large gains of pTRM and small losses of NRM.

[16] The pattern changes for the final steps, 565°–580°C. The 565° and 572°C steps are modeled in Figure 2. Thermal demagnetization proceeds as before, but in the field-on step at 565°C, starting from thermal demagnetization initial state 12″, the r value at 13 exceeds the total TRM and tracks back down the TRM blocking master curve from 13′ to 13″ during field cooling to T_o. The pTRM gained is calculated as Δr_o between 13″ and 12″. However, r_o at 13″ equals the total TRM, and r_o at 12″ is the NRM remaining. Thus the NRM and pTRM results for 565°C and higher T have ideal SD-like behavior, the pTRM gained exactly restoring the NRM lost. The physical behavior in detail is far from SD-like, but the net result mimics ideal Thellier behavior.

[17] The Arai plot of Figure 3a shows clearly the three regimes. Below 540°C the pTRM that would be produced starting from a demagnetized state is less than the NRM remaining after thermal demagnetization. Thus the initial state dictates no net pTRM gain. Between 540°C and 563°C the NRM continues to thermally demagnetize slowly, but the amount of magnetization produced in each field-on step much exceeds the remaining NRM, and there is a large net pTRM gain. From 565° to 580°C the equilibrium magnetization in H_o at T is greater than the room temperature TRM. M reequilibrates during field

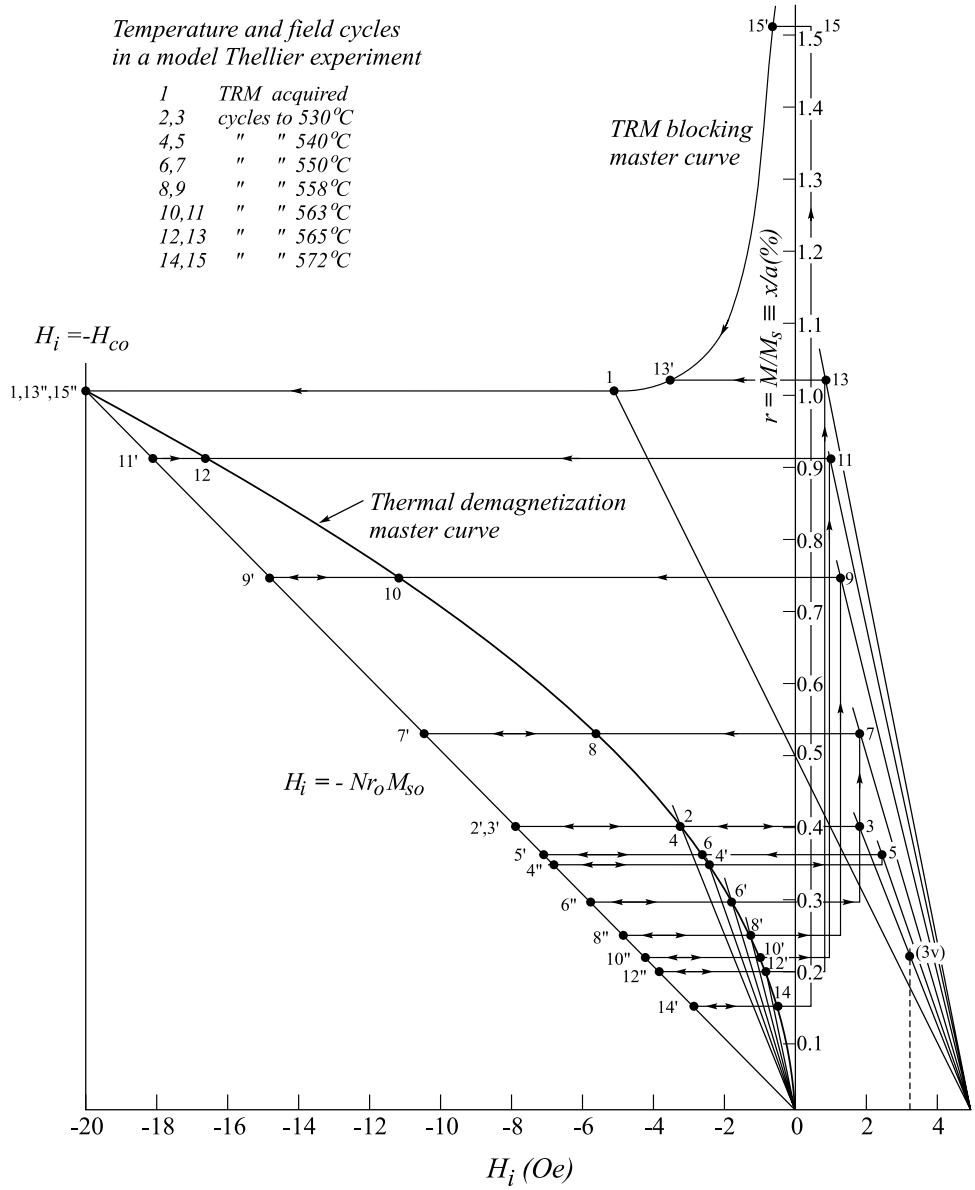

Figure 2. A Thellier model diagram from which natural remanent magnetization (NRM) remaining and pTRM gained can be calculated for a sequence of zero-field and in-field heating-cooling cycles (here to $T = 530°C, \ldots, 572°C$) with specified experimental parameters (here $H_{co} = 2$ mT or 20 Oe, $H_o = 0.5$ mT, and $n = 2$). The sets of inclined lines of negative slope (e.g., the one labeled $H_i = -Nr_oM_{so}$) are demagnetizing lines at various T. The vertical lines (e.g., the one labeled $H_i = -H_{co}$) or segments are sections of internal field loops. The thermoremanent magnetization (TRM) blocking and thermal demagnetization master curves are from *Dunlop and Xu* [1994]. For the detailed procedure used to find the numbered intersection points, see the text.

cooling to the TRM value, and the Arai plot rejoins the ideal SD line.

[18] Although intricate at first sight, Thellier model diagrams like Figure 2 are easy to use. The TRM and thermal demagnetization master curves are universal, once the model parameters have been chosen. The ascending loops and self-demagnetization relations are straight lines that are easily computed for a given set of T steps. The calculations can be carried out mathematically without recourse to a model diagram, but the graphical approach gives more insight.

[19] Figure 3a also shows the results of calculations using a distribution of coercivities, $f(H_{co})$. A single microcoercivity was assumed for individual grains, but the coercive force was allowed to vary from grain to grain following an exponential relation. There is considerable smoothing compared to the piecewise linear Arai plot for a single value of H_{co}, but the three regimes of behavior are still recognizable. Thermal demagnetization with minor pTRM gain dominates at low to intermediate T, pTRM gain outstrips NRM loss at intermediate to high T, and quasi-ideal behavior occurs for T approaching T_C. Although the method of introducing a

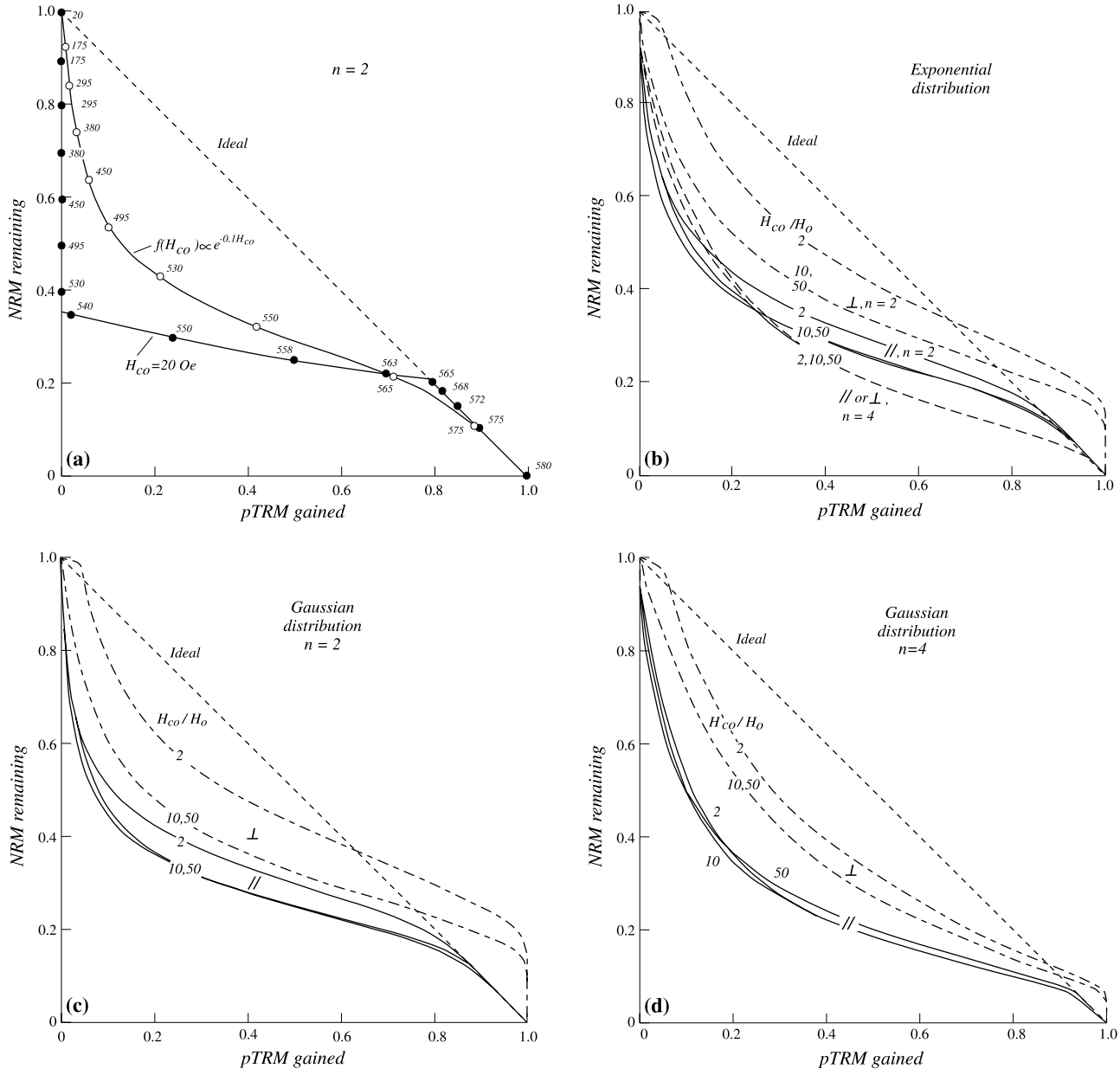

Figure 3. (a) Arai plots showing results of the double heatings modeled in Figure 2 (solid circles) and results of similar calculations with grain microcoercivities distributed exponentially (open circles). Heatings up to 530°C produce no net pTRM, only loss of NRM. Most pTRM is gained between 540°C and 565°C, with little loss of NRM. NRM loss is balanced by pTRM gain (quasi-ideal behavior) above 565°C. (b) Results of Thellier double-heating calculations for an exponential distribution of microcoercivities $f(h_{co})$ within grains when $n = 2$ and 4. If pTRMs are parallel to the NRM, the curves are strongly convex down and display the same three regions seen in Figure 3a. If pTRMs are perpendicular to the NRM, there is less deviation from the ideal single-domain (SD) line, and the results overshoot the line rather than joining it at the highest temperatures. (c) Calculated Arai plots for a Gaussian distribution $f(h_{co})$ with $n = 2$. (d) Calculated Arai plots for a Gaussian distribution $f(h_{co})$ with $n = 4$. Compared to Figure 3c, there is more sagging of the perpendicular set of curves below the ideal line but less overshooting at high temperatures.

coercivity distribution is crude and physically not very realistic, the resulting Arai plot closely resembles the predictions of more sophisticated modeling (section 3) and experimental data (section 4).

3. Theory for a Distribution of Microcoercivities

[20] In section 2 we assumed that energy barriers produced by defects that pin walls are identical and symmetrical, resulting in a single microcoercivity and a rectangular $M(H_i)$ loop. We thereby gained an appreciation of the various processes at play in interwoven thermal demagnetization and pTRM steps, where the final state of one step is the initial state for the next. However, in real grains, defects are neither identical nor regularly spaced, so that E_w is an irregular function of x. Then we must deal with a distribution of microcoercivities $f(h_{co})$ within individual grains.

[21] *Xu and Merrill* [1989] showed that for a very large number of randomly distributed defects, $f(h_{co})$ is a Gaussian normal distribution. On the other hand, *Dunlop* [1983] analyzed experimental alternating field demagnetization curves of MD rocks and deduced an approximately exponential distribution $f(h_{co})$. Our calculations therefore used two different possibilities, an exponential distribution

$$f(h_{co}) = (1/H_{co}) \exp(-h_{co}/H_{co}) \tag{4}$$

and the positive half of a Gaussian distribution

$$f(h_{co}) = (2/\pi H_{co}) \exp\left(-h_{co}^2/\pi H_{co}^2\right), h_{co} \geq 0. \tag{5}$$

In either case, H_{co} is the mean of $f(h_{co})$.

[22] The mean magnetization M is calculated as an integral over the part of the distribution $f(h_{co})$ activated in a given process (see algorithms below):

$$M = \int m(h_{co})\, f(h_{co}) dh_{co}, \tag{6}$$

where $m(h_{co})$ is the magnetization due to displacement of an individual wall pinned by microcoercivity h_{co}. An implicit assumption in determining M from equation (6), using the expressions for $m(h_{co})$ derived by *Dunlop and Xu* [1994], is that different walls in the same grain can be treated as independent. This is clearly an oversimplification because the self-demagnetizing field is determined by the net magnetization due to displacements of all the walls. One approach is to solve a set of integral equations corresponding to different walls in a grain [*Xu and Dunlop*, 1993], but this is possible only in certain limited situations. An alternative is to postulate two populations of walls, hard (strongly pinned) and soft (loosely pinned). The hard walls can be treated as independent, while the soft walls provide negative induced magnetizations that partially screen or offset the hard remanence. A simple screening factor used successfully by *Dunlop and Kletetschka* [2001] to predict TRM intensities of MD magnetite and hematite is $\alpha = (1 + N\chi_i)^{-1}$, where χ_i is internal-field susceptibility. In principle, all the NRM and pTRM intensities we calculate below should be reduced by a factor α.

[23] A graphical representation is now too intricate to be useful, and the calculations proceed numerically. First, we deal with the case where $\mathbf{H_o}$ (=$\mathbf{H_L}$, the laboratory field) and the resulting pTRMs m_{ptrm} are parallel to the NRM. Later, we will treat the case of $\mathbf{H_o}$ perpendicular to NRM. All other experimental possibilities are a combination of these two. As an NRM we again assume a total TRM, produced in nature by a field $\mathbf{H_A}$ or for our Thellier simulation experiments by a laboratory field. The algorithm uses theoretical expressions derived by *Dunlop and Xu* [1994] and *Xu and Dunlop* [1994], as follows.

[24] 1. Calculate NRM, i.e., total TRM:

$$m_{nrm} = \left[n/(n-1)^{1-1/n}\right]\left(H_o^{1-1/n} h_{co}^{1/n}/N\right)$$

(field blocking) or

$$m_{nrm} = h_{co}/N$$

(wall reequilibration), whichever is smaller. Then $M_{nrm}(T_o) = \int m_{nrm}(h_{co}, T_o)\, f(h_{co})\, dh_{co}$.

[25] 2. Calculate thermal demagnetization to temperature T_i:

$$m_{nrm} = \left[n/(n-1)^{1-1/n}\right]\left(H_o^{1-1/n} h_{co}^{1/n}/N\right)$$

(field blocked) or

$$m_{nrm} = (h_{co}/N)\, \beta^{n-1}(T_i)$$

(unblocked, reequilibration), whichever is smaller. Then $M_{nrm}(T_i) = \int m_{nrm}(h_{co}, T_i)\, f(h_{co})\, dh_{co}$.

[26] 3. Calculate partial TRM acquisition from T_i to T_o: If

$$H_o < h_c(T_i) = h_{co}\, \beta^n(T_i),$$

then m_{nrm} is unchanged from the previous step. If

$$H_o > h_c(T_i),$$

then

$$m'_{nrm} = \left[n/(n-1)^{1-1/n}\right]\left(H_o^{1-1/n} h_{co}^{1/n}/N\right)$$

(field blocking),

$$m'_{nrm} = [H_o - h_{co}\, \beta^n(T_i)]/[N\, \beta(T_i)]$$

(isothermal blocking) or

$$m'_{nrm} = h_{co}/N$$

(wall reequilibration), whichever is smallest. Next, calculate

$$M'_{nrm}(T_i) = \int m'_{nrm}(h_{co}, T_i)\, f(h_{co}) dh_{co}$$

$$M_{ptrm}(T_i) = M'_{nrm}(T_i) - M_{nrm}(T_i).$$

The pTRM is calculated according to the prescription of the Thellier method.

[27] 4. For $T_{i+1} > T_i$, repeat steps 2 and 3. Note that initial state information is built in.

[28] Now we treat the case of $\mathbf{H_o}$ perpendicular to NRM.

[29] 1. Perform step 1 as above.

[30] 2. Perform step 2 as above.

[31] Step 3 is somewhat different because the pTRM is now perpendicular to the NRM and can be measured directly. The previously used differencing procedure between steps 3 and 2 is unnecessary.

[32] 3. Calculate partial TRM acquisition from T_i to T_o: If

$$H_o < h_c(T_i) = h_{\rm co}\,\beta^n(T_i),$$

then $m_{\rm ptrm} = 0$. If

$$H_o > h_c(T_i),$$

then

$$m_{\rm ptrm} = \left[n/(n-1)^{1-1/n}\right]\left(H_o^{1-1/n}h_{\rm co}^{1/n}/N\right)$$

(field blocking),

$$m_{\rm ptrm} = [H_o - h_{\rm co}\,\beta^n(T_i)]/[N\,\beta(T_i)]$$

(isothermal blocking), or

$$m_{\rm ptrm} = h_{\rm co}/N$$

(wall reequilibration), whichever is smallest.

$$M_{\rm ptrm}(T_i) = \int m_{\rm ptrm}(h_{\rm co}, T_i)\, f(h_{\rm co})\, dh_{\rm co}.$$

[33] Calculated results for various model parameters (n = 2 or 4, H_o = 0.1 mT, and $H_{\rm co}/H_o$ = 2, 10, or 50), experimental modes (parallel or perpendicular), and $f(h_{\rm co})$ (exponential or Gaussian) appear in Figures 3b–3d. All the curves have the same general aspect, which resembles that of the crude exponential simulation of Figure 3a. For the parallel field configuration, three regions are again seen: Thermal demagnetization dominates at low to intermediate T; pTRM acquisition dominates at intermediate to high T; and quasi-ideal behavior occurs as $T \rightarrow T_{\rm C}$. When pTRM is produced perpendicular to NRM, the third region changes: The data are predicted to overshoot the ideal SD line on the Arai plot.

[34] The reason for this change in behavior can be appreciated by referring to Figure 2. At the highest T steps, 565° and 572°C, the pTRM produced in the field-on step was actually equal to the total TRM. However, the pTRM calculated by the Thellier prescription was reduced by subtracting the residual NRM. This is necessary because experimentally the magnetizations are parallel and cannot be distinguished. Following this procedure, the sum NRM plus pTRM will always be equal to total TRM, ensuring that points on the Arai plot are forced to follow the ideal line. However, in the perpendicular configuration, pTRM can be measured separately from NRM, so that pTRM for the highest T steps approaches or equals total TRM, as seen in Figures 3b–3d.

4. Experimental Thellier Results

[35] To make samples, large natural crystals of magnetite were crushed and separated into coarse and fine fractions. Five powders, with mean grain sizes of ~135, 20, 6, 1, and 0.6 μm, were used in our experiments. Low-temperature saturation remanence gave a sharp magnetite Verwey transition at 110–115 K. Weak field susceptibility χ dropped to near zero just below the magnetite Curie point of 580°C in all samples. The 1 and 0.6 μm grains also had a very small signal due to hematite, but their cooling curves were lower than the heating curves, showing that oxidation occurred during heating above 580°C and not during preparation of the magnetites. The $\chi - T$ curves changed from T independent (MD, controlled by self-demagnetization) for the large grains to ramps with a Hopkinson peak for the finer grains. The magnetites were dispersed in CaF_2 (~1% by weight), packed into individual quartz capsules, which were sealed under vacuum and annealed at 650°–700°C to relieve internal stress. Postannealing hysteresis parameters [*Dunlop*, 2002, Figures 3 and 8d] range from MD ($M_{\rm rs}/M_s$ = 0.012, $H_{\rm cr}/H_c$ = 11.6 for 135 μm grains) to PSD ($M_{\rm rs}/M_s$ = 0.15, $H_{\rm cr}/H_c$ = 2.4 for 0.6 μm grains).

[36] Thellier experiments using 14–18 temperature steps were carried out with $\mathbf{H_L}$ both parallel and perpendicular to NRM. A Schonstedt furnace was at first used, but the twin requirements of high resolution (±1°C near $T_{\rm C}$ for the 135 μm sample, Figure 7) and exact repeatability of T_i in field-off and field-on steps were difficult to satisfy, owing to T gradients and thermal inertia, which can lead to overshooting. The Thellier experiments were therefore rerun using a water-cooled noninductive quartz resistance furnace. With patient fine-tuning of the current it was possible to achieve target temperatures with the necessary precision and repeatability. Comparing results from the two furnaces, Arai curve shapes were very similar, but nominal T_i values at specific points along a curve differed somewhat because of different sample positioning relative to the thermocouple. In the case of the 135 μm sample, only the quartz furnace data are reported.

[37] The NRM in each experiment was a total TRM. The field $\mathbf{H_o}$ in field-on heating steps was identical in strength (0.1 mT) to that used to produce TRM. Thus the laboratory field $\mathbf{H_L}$ is the same as the "ancient" field "$\mathbf{H_A}$," apart from orientation in the perpendicular experiments, and the ideal SD line on the Arai plot has slope −1.

[38] Results for the 135 μm sample are given in Figure 4a. The "MD theory" curve is the result for an exponential $f(h_{\rm co})$ with n = 4 in the parallel configuration (Figure 3b), chosen because it gives the best overall fit to the parallel experimental data. A Gaussian $f(h_{\rm co})$ with n = 4 (Figure 3d) gives a fit of similar quality. Theoretical curves for n = 2 give too steep an initial descent. The theoretical curve for a Gaussian $f(h_{\rm co})$ with n = 4 in the perpendicular configuration (not shown in Figure 4a) gives a reasonable fit to the perpendicular data, except that the data do not overshoot the ideal line as $T \rightarrow T_{\rm C}$. Most of the information comes from T_i steps ≥500°C in the parallel experiment and from T_i steps ≥450°C in the perpendicular experiment. About 2/3 of

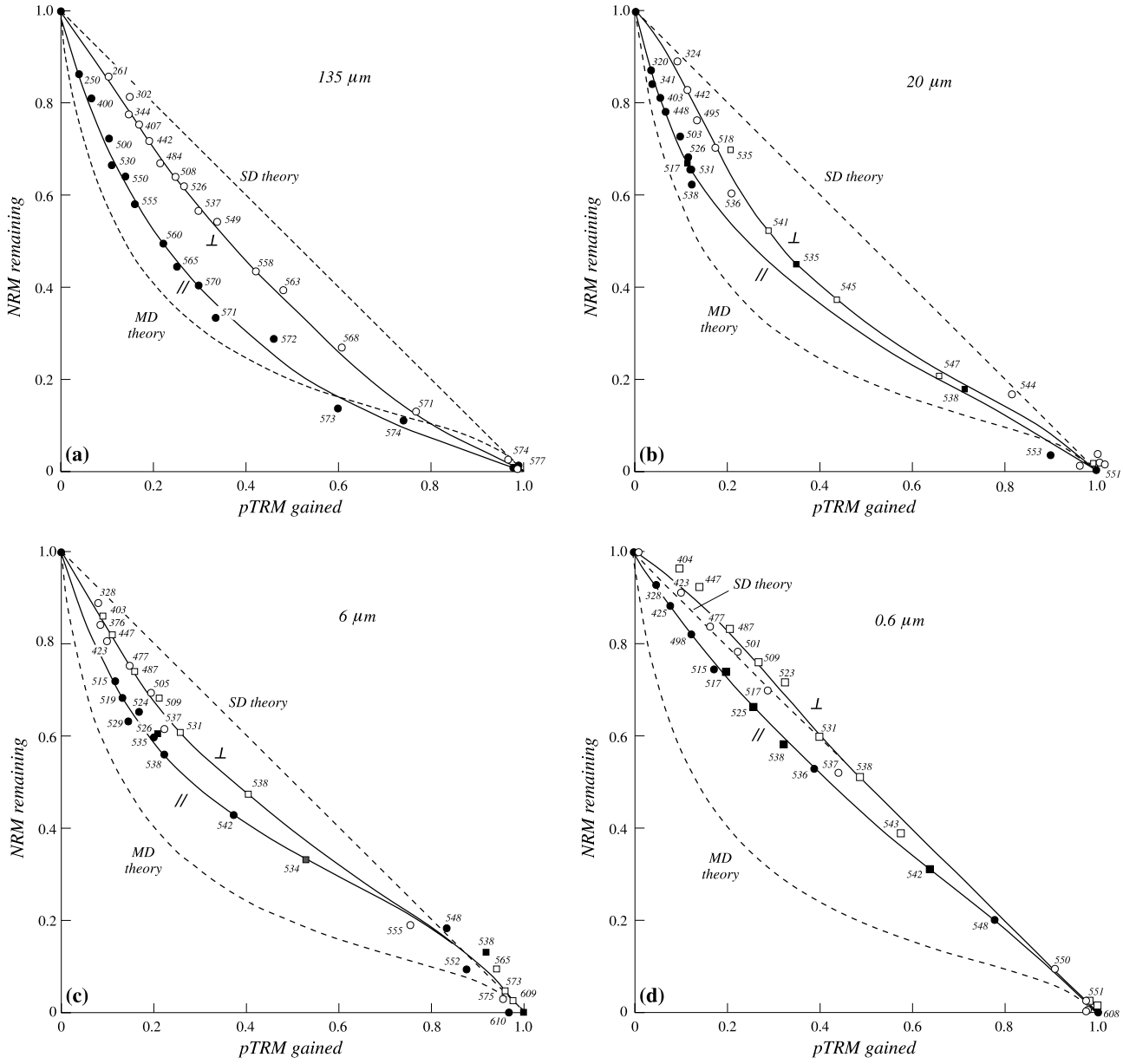

Figure 4. (a) Results of Thellier simulation experiments for the 135 μm magnetite. A field $\mathbf{H_L}$ = 0.1 mT was used to produce the initial "NRM" (a total TRM) and all pTRMs. In the perpendicular experiment the sample was rotated 90° after NRM production. The results of both parallel and perpendicular experiments sag much below the ideal line predicted by SD theory and agree semiquantitatively with the predictions of MD theory for n = 4 (Figures 3b and 3d). (b) Experimental Thellier results for the 20 μm magnetite. The initial descent of the curves is almost as steep as for the 135 μm grains, but there is less deviation overall from ideal behavior because the middle- to high-temperature part of each curve is inflected and approaches the SD line. (c) Experimental results for the 6 μm magnetite. These strongly inflected curves illustrate the three predicted regions of NRM loss, pTRM gain, and quasi-ideal behavior (Figures 3a–3d). (d) Experimental Thellier results for the 0.6 μm magnetite. These results, particularly the perpendicular data, approach ideal SD behavior although the average grain volume is 100–1000 times that of an SD grain of critical size. Circles and squares in Figures 4b–4d are data from the quartz resistance and Schonstedt furnaces, respectively.

the pTRM blocking temperatures are ≥570°C (parallel) or ≥550°C (perpendicular). This concentration of high blocking (but not unblocking) temperatures is characteristic of MD grains.

[39] The parallel data up to 571°C follow a straight line, while the deviations from 572° to 580°C resemble the effects of sample alteration [e.g., *Kosterov and Prévot*, 1998]. One could make a least squares fit to the 10 data points from 250° to 571°C, which represent 53% of the NRM and give a highly acceptable f value [*Coe et al.*, 1978]. The points are evenly spread, yielding a good g value [*Coe et al.*, 1978]. The resulting $\mathbf{H_A}/\mathbf{H_L}$ value, 1.8 (Table 1),

Table 1. Slopes and Fractions of NRM Utilized for Best Fitting Straight Lines to Portions of the Arai Plot Data

Grain Size, μm	Mode	*T* Range, °C	Fraction of NRM	|Slope|
135	parallel	250–565	0.42	2.0
	parallel	250–571	0.53	1.8
	parallel	530–571	0.33	1.57
	perpendicular	261–558	0.32	1.37
	perpendicular	484–571	0.54	0.99
	perpendicular	537–571	0.44	0.93
20	parallel	320–538	0.22	2.6
	perpendicular	324–536	0.30	2.45
6	parallel	515–538	0.16	1.5
	perpendicular	328–531	0.28	1.58
0.6	parallel	328–538	0.27	1.25
	parallel	515–542	0.44	0.96
	parallel	328–551	0.92	0.96
	perpendicular	423–551	0.91	1.00

overestimates the "ancient" field by 80%. *Shcherbakov and Shcherbakova* [2001] reported overestimates of up to 60% by forcing linear fits on low-T_i data in Arai plots of natural MD samples and even larger than this for synthetic MD magnetites. *McClelland et al.* [1996] found similar deviations for 5–150 μm magnetites.

[40] The perpendicular data deviate much less from the ideal 1-1 line. Slopes are also close to 1 over some data ranges (Table 1). Performing the Thellier experiment with $\mathbf{H_L}$ perpendicular to the NRM [*Kono and Ueno*, 1977] thus has real advantages, although it is not easily done with commercial furnaces and standard cylindrical paleomagnetic cores.

[41] Figures 4b and 4c illustrate the results for the 20 and 6 μm samples, respectively; 20 μm is at the lower limit of "truly MD" behavior (governed by self-demagnetization), while 6 μm is within the "pseudo-single-domain" range where various properties of magnetite imply a SD-like fraction of remanence [e.g., *Dunlop et al.*, 2004]. Nevertheless, the results for the two samples are similar. The inflected Arai curves bear a strong resemblance to theoretical curves (Figures 3a–3d), while lying closer on average to the ideal SD line than the 135 μm data (Figure 4a). The perpendicular data are fairly similar to the parallel data, and for the 20 μm sample they lie farther from the ideal line than the 135 μm data. A linear fit to the perpendicular data at lower temperatures would give only a slightly improved estimate of H_A compared to a similar fit to the parallel data for both the 6 μm and 20 μm samples, and the fraction of NRM utilized would be much less than for the 135 μm sample (Table 1). Partial TRM acquisition is concentrated in a narrow range between 535° and 550°C, somewhat lower than for true MD grains. There is little or no overshooting of the ideal SD line as $T_i \rightarrow T_C$.

[42] The results for the 0.6 and 1 μm samples approach ideal SD behavior. The 0.6 μm data are shown (Figure 4d). Data for the parallel experiment sag only slightly below the 1-1 line, and for the perpendicular experiment they lie on or even above the line. Nevertheless, a linear approximation to the lower-T_i data for the parallel mode overestimates H_A by 25% (Table 1).

5. Discussion of Thellier Results

[43] In every case a Thellier experiment with the laboratory field perpendicular to the NRM gave closer-to-ideal Arai plots than the parallel experiment. The reason is that pTRM gained at T_i in the perpendicular case is greater than pTRM calculated for the same T_i in the parallel case. For SD grains any pTRM acquired at T_{i-1} is completely erased in the demagnetization step to T_i. For MD grains, there is always a residual pTRM tail which is not erased and is added to the NRM [*Dunlop and Özdemir*, 2001, Figure 5]. In the parallel experiment, following the usual methodology, this residual is subtracted in calculating pTRM gained. In the perpendicular experiment the residual is orthogonal to NRM and is included in the newly produced pTRM rather than being subtracted. These different procedures and results are forced on us by the fact that the pTRM residual is parallel to NRM in one case but perpendicular to it in the other.

[44] As grain size increases from near SD size (0.6 and 1 μm) to large MD (135 μm), the shape of the Arai plot evolves from nearly ideal SD linearity to downward convexity with a mid range inflection point. The parallel data are compared in Figure 5. The 135 μm data agree most closely with theoretical predictions and deviate most from the SD line. However, the 6 μm results show the most marked mid range inflection, delineating the predicted separation into NRM loss, pTRM gain, and ultimate ideal behavior regimes. The higher-T_i data for the 135 μm sample are scattered because of the difficulty of repeating steps with ±0.5°C accuracy, and an inflected curve is not ruled out.

[45] Gaussian or exponential distributions with an $h_c(T)$ index (equation (3)) of $n = 4$ give the best agreement with both parallel and perpendicular results for the 135 μm magnetites. A less rapid decrease of h_c with T, e.g., $n = 2$, gives definitely inferior fits. The data for perpendicular applied fields approach but do not overshoot (or only marginally overshoot) the ideal SD line (Figures 4a–4d). Data for natural MD magnetite do in some cases show overshooting at the highest T_i steps (D. J. Dunlop et al., Thellier paleointensity experiments on mineral separates, submitted to *Journal of Geophysical Research*, 2004, hereinafter referred to as Dunlop et al., submitted manuscript, 2004).

[46] Why are MD Arai plots convex? Our theory predicts that multidomain TRM will begin to demagnetize well below its blocking temperature T_B or the mean of its range of T_B. We also predict a threshold temperature below which little or no pTRM is acquired. Both effects are ultimately due to the internal self-demagnetizing field, which causes

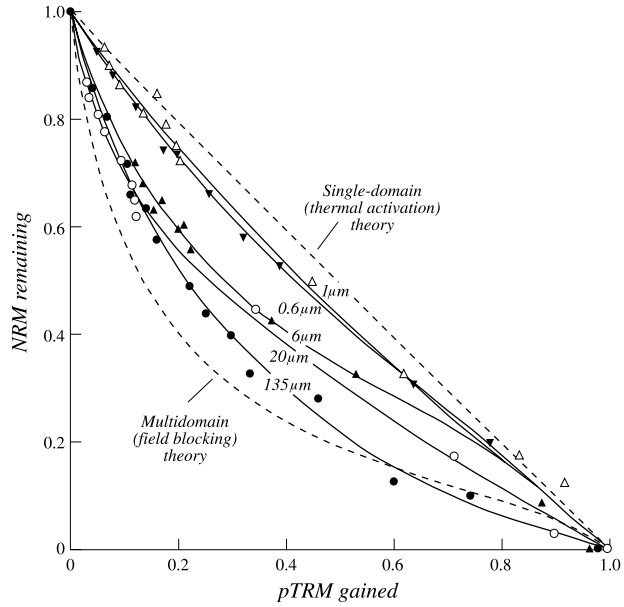

Figure 5. Comparison of results of the parallel Thellier experiment over the range from nearly SD (0.6 and 1 μm) to large MD grain sizes. Curves with the inflected shape predicted by field blocking theory are most prominent for small (6 μm) rather than large MD grains. The theoretical MD curve uses an exponential distribution $f(h_{co})$ with $n = 4$.

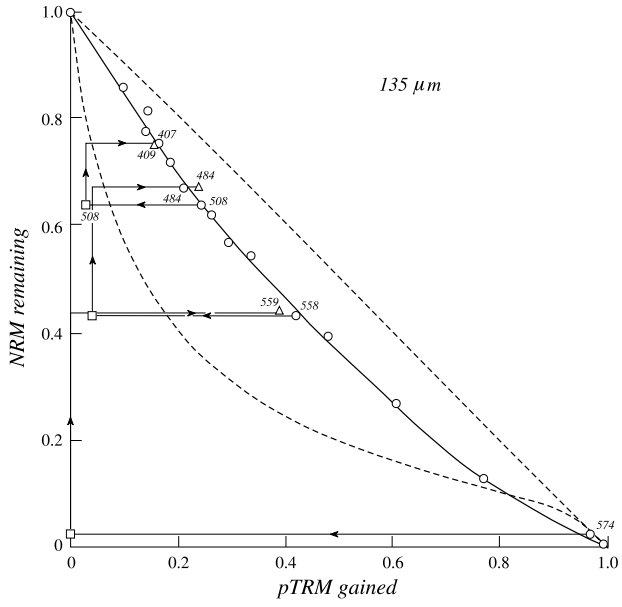

Figure 7. Tail checks (squares) and pTRM checks (triangles) carried out as part of the perpendicular Thellier experiment for the 135 μm sample. Although two of the three tail checks are negative, showing undemagnetized pTRM residuals, the pTRM checks are acceptable, showing that the convex Arai plot is reproducible. Circles are original data.

walls to reequilibrate during heating toward a state of lower magnetization. The effects are well illustrated in a Roquet plot [*Roquet and Thellier*, 1946] of the 135 μm data, showing NRM and pTRM as explicit functions of T_i (Figure 6). For SD grains the two curves would be mirror images, any NRM loss being exactly replenished by pTRM gain. For MD grains like ours, NRM decreases quite rapidly with heating, while pTRM acquisition is more sluggish. The result is a convex NRM-pTRM graph.

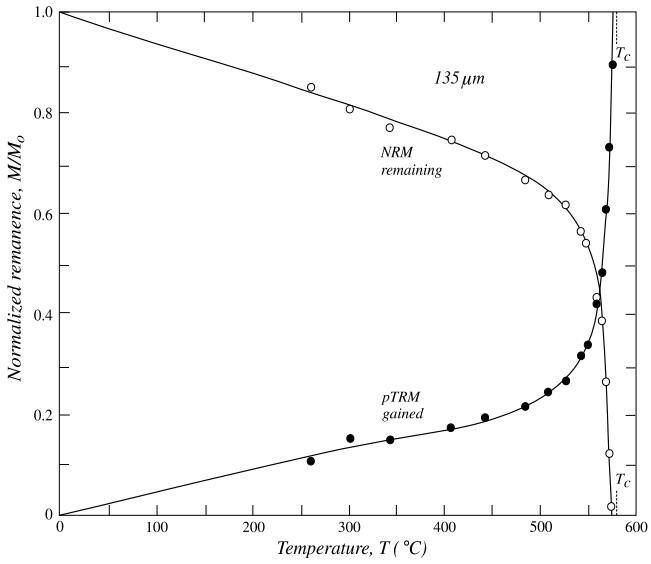

Figure 6. Experimental Thellier results for the 135 μm magnetite in the form of a Roquet plot of NRM and pTRM separately as functions of *T*. NRM is lost more rapidly than pTRM is gained, producing nonideal Arai plots.

6. Experiments With pTRM Checks and Low-Temperature Demagnetization Pretreatment

[47] Figure 7 illustrates pTRM checks and pTRM tail checks carried out as part of the perpendicular Thellier experiment for the 135 μm magnetites. Two additional steps are involved. A third heating-cooling in zero field to T_i to check for undemagnetized pTRM (the tail check [*Riisager and Riisager*, 2001]) was followed by an in-field heating-cooling to replicate pTRM at a lower temperature. Two of the three tail checks were negative, revealing pTRM residuals. In spite of this all three pTRM checks were positive and reproduced earlier pTRMs within acceptable error bounds. Thus the curved Arai plots are not due to chemical alteration (obvious for our vacuum-sealed samples, not obvious for rocks in general) but are a reproducible phenomenon with a physical cause, namely, self-demagnetization.

[48] It would be extremely helpful if a method could be devised to make MD Thellier results more ideal and SD-like. One approach is to subject the NRM and all pTRMs to low-temperature demagnetization (LTD), zero-field cycling through the magnetite Verwey transition and isotropic point around 120–130 K. LTD unpins domain walls and may also trigger nucleation (see discussion given by *Dunlop* [2003]), reducing MD remanence. The procedure is laborious and was not particularly successful for our 135 μm sample (Figure 8). For the parallel experiment the data do not move much closer to the ideal line, although the curvature decreases substantially. The average slope of

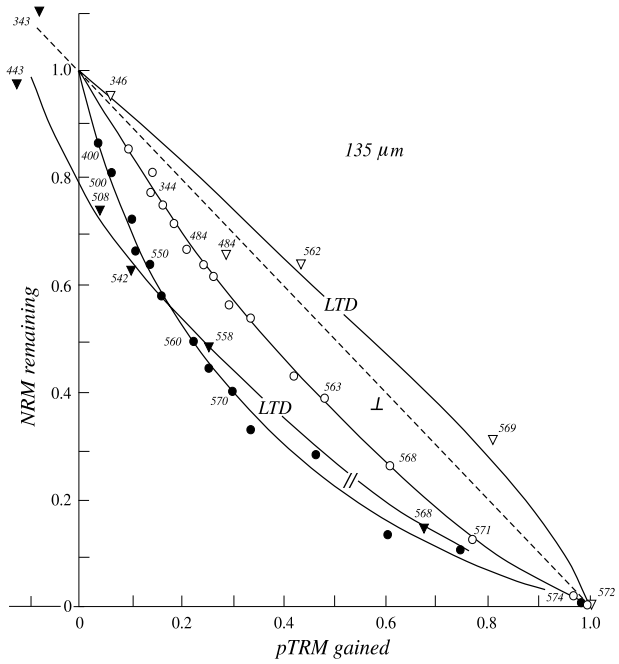

Figure 8. An attempt to ameliorate the nonlinearity of MD Thellier data by low-temperature demagnetization (LTD) pretreatment. The improvement in linearity does not justify the laborious LTD technique.

the data taken as a whole is now <1. The perpendicular post-LTD data are scattered, and most lie above the ideal line. In both cases a narrower range of T_i is usable after LTD compared to before. *McClelland et al.* [1996] likewise found LTD ineffectual as a pretreatment.

7. Paleomagnetic Implications

[49] *Néel*'s [1955] theory has its shortcomings [*Shcherbakov and Shcherbakova*, 2001]. The $H_o^{1-1/n}$ field dependence of TRM (algorithm, section 3) is relevant to paleointensity determination, which assumes linearity in H_o. The problem is minor if H_L is similar to H_A, as in our simulations, but it could be important if H_A and H_L are very different. For $n = 4$, which gave best fit of theory to experiment for the 135 μm magnetite, TRM intensity would theoretically vary $\sim H_o^{3/4}$ instead of $\sim H_o$. Also, for weak fields like the Earth's, thermal fluctuations may unblock TRM at a temperature T_{Bf} below T_{B} predicted by field blocking. T_{Bf} can be calculated exactly for SD grains, but for MD grains, T_{Bf} involves the unknown fluctuation field at T_{Bf}. Thermal fluctuations will tend to linearize the field dependence and to reduce T_{B} and T_{UB} values by perhaps 10°–20°C. The overall picture of reequilibration driven by self-demagnetization remains valid, and the shapes of the Arai plots should change very little, although absolute T_i values will shift along the curves.

[50] One interesting result of our extension of *Néel*'s [1955] theory is a predicted threshold for net pTRM gain in a parallel Thellier experiment. In a real paleointensity run, NRM is usually at some angle other than 0° to $\boldsymbol{H}_{\mathbf{L}}$, but it might still be useful to try to establish a rough pTRM threshold temperature for a sample set (D. N. Thomas, personal communication, 2004). Below-threshold data would be automatically rejected from use in paleointensity estimates. Whether the labor of supplementary pTRM experiments would justify the potential benefits remains to be seen.

[51] In the discussion of section 5 we emphasized the evolution of Arai plots: from strongly curved but consistent with MD theory for the largest grains to quasi-linear and consistent with SD theory for the finest grains. A more practical question is which, if any, of these plots can be made to yield accurate paleointensities. LTD pretreatment (section 6) is of little help. A crude procedure would be to use only the initial and final points [*Levi*, 1977], in essence a one-step Thellier experiment, but this ignores the reality of secondary remanences, mixtures of MD and other size grains, and mixtures of minerals. However, even in our most nonlinear Arai plots, there were quasi-linear regions with slopes close to 1 (Table 1). Most promising were data from perpendicular experiments in middle- to high-T ranges: 484°–571°C and 537°–571°C (135 μm (Figure 4a), slopes 0.99 and 0.93, respectively) and 423°–551°C (0.6 μm (Figure 4d), slope 1.00). The NRM fractions used were quite large (0.54, 0.44, and 0.91). Mid-T fits for the 6 and 20 μm samples, with their heavily inflected curves, gave much too high estimates for both parallel and perpendicular modes but would have been rejected in paleomagnetic practice [*Biggin and Thomas*, 2003] on the basis of their small f values of 0.16–0.30 (Table 1).

[52] For the 0.6 μm sample in the parallel experiment a fit to lower-T points (328°–538°C) gave a slope of 1.25. This is exactly the average reported by *Calvo et al.* [2002] for their best Mount Etna lava samples, containing only magnetite and giving apparently reliable, quasi-linear Arai plots. The authors ascribed the high slopes "to the fact that the low- to medium-temperature pTRMs, which represent a significant fraction of the total TRM, seem to be carried by small MD particles." On the other hand, somewhat higher-T points (515°–542°C) for our 0.6 μm sample gave an acceptable slope of 0.96. The former fit would have been rejected in any case on the basis of its low f of 0.27, while the latter has a marginally acceptable f of 0.44. The criterion $f > \sim 0.5$ proposed by *Biggin and Thomas* [2003] thus seems to be effective.

[53] An even higher f value of 0.92 can be achieved by using all the parallel points for our 0.6 μm sample from 328° to 551°C. The quality of the linear fit is much poorer, but the slope of 0.96 is acceptable (Table 1). *Hill and Shaw* [2000] also found that a line of best fit through all points, regardless of curvature, gave the closest agreement with the known field for the 1960 Kilauea (Hawaii) lava flow. In the case of our 0.6 μm sample the best result of all uses all the perpendicular data from 423° to 551°C, giving a slope of 1.00 and $f = 0.91$ (Table 1), with all data falling very close to an ideal straight line (Figure 4d).

[54] In a perpendicular experiment on the 135 μm sample (Figure 7) we found that pTRM checks reproduced lower-T pTRMs in spite of strong curvature of the Arai plot and negative pTRM tail checks, both due to MD grains. On this evidence, pTRM checks and pTRM tail checks do succeed in separating MD and alteration effects. However, in a companion paper on natural MD magnetites (Dunlop et al., submitted manuscript, 2004), pTRM tail checks in parallel experiments are often null even in the presence of MD grains [see also *Yu and Dunlop*, 2003], and pTRM

checks increasingly overshoot prior pTRMs as T increases, as found also by *Biggin and Thomas* [2003]. Furthermore, in a Thellier experiment with the field at an arbitrary angle to sample NRM vectors, any pTRM tail will shift the effective NRM direction measured after zero-field steps toward $\boldsymbol{H}_{\mathbf{L}}$ in exactly the same way as a CRM produced by alteration during laboratory heating. We advise caution in interpreting pTRM and tail checks in the light of our present incomplete understanding of MD Thellier behavior.

[55] This paper deals only with magnetite, but primary titanomagnetites that have escaped deuteric or low-temperature oxidation commonly occur in MD sizes in volcanic rocks. Thellier paleointensity determination on unoxidized TM60 (titanomagnetite with 60 mol% Ti) is generally unsuccessful because of its low coercivities, Curie point, and blocking/unblocking temperatures. However, our theoretical treatment could readily be adapted to TM60 by changing material properties such as M_s, T_C, and n.

8. Conclusions

[56] A straightforward theory, based on field blocking of TRM and pTRM and wall reequilibration by self-demagnetizing fields, explains most features of MD Thellier results. Arai plot shapes and distributions of blocking and unblocking temperatures are accounted for. A threshold temperature is predicted below which no net pTRM is produced.

[57] Experimentally, magnetites as large as 1 μm have nearly linear Thellier plots that give acceptable paleointensities. Larger grains have convex down plots whose curvature increases with increasing grain size. However, it is sometimes possible to find linear regions at intermediate T that yield acceptable paleointensities. Using only lower-T points gives paleointensity overestimates of up to 100% for ~100 μm grains. A minimum f value of ~0.5 [*Biggin and Thomas*, 2003] is effective in rejecting spurious values.

[58] If there is no chemical alteration on heating, as for our samples, pTRM tail checks are negative (undemagnetized pTRM residuals), but pTRM checks are positive. Thus the curved Arai plots are reproducible: Physical rather than chemical effects are involved.

[59] A Thellier experiment with the laboratory field perpendicular to the NRM [*Kono and Ueno*, 1977] gives closer-to-ideal Arai plots and improved paleointensity estimates compared to an experiment with field parallel to NRM. The perpendicular method can, in principle, use single heatings, since NRM and pTRM are orthogonal, but double heatings are preferable because they allow pTRM tails to be measured.

[60] **Acknowledgments.** Helpful reviews by Neil Thomas and Andrei Kosterov led to a deeper appreciation of the practical aspects of this work. Sample characterization was done at the Institute for Rock Magnetism, University of Minnesota, which is supported by the Earth Sciences Division of NSF and the Keck Foundation. Thellier experiments were done at the University of Toronto. This research was supported by the Natural Sciences and Engineering Research Council of Canada (NSERC) grant A7709 to D.J.D.

References

Biggin, A. J., and D. Neil Thomas (2003), The application of acceptance criteria to results of Thellier palaeointensity experiments performed on samples with pseudo-single-domain characteristics, *Phys. Earth Planet. Inter.*, *138*, 279–287.

Calvo, M., M. Prévot, M. Perrin, and J. Riisager (2002), Investigating the reasons for the failure of palaeointensity experiments: A study on historical lava flows from Mt. Etna (Italy), *Geophys. J. Int.*, *149*, 44–63.

Coe, R. S. (1967), Paleointensities of the Earth's magnetic field determined from Tertiary and Quaternary rocks, *J. Geophys. Res.*, *72*, 3247–3262.

Coe, R. S., C. S. Grommé, and E. A. Mankinen (1978), Geomagnetic paleointensities from radiocarbon-dated lava flows on Hawaii and the question of the Pacific nondipole low, *J. Geophys. Res.*, *83*, 1740–1756.

Dunlop, D. J. (1983), Determination of domain structure in igneous rocks by alternating field and other methods, *Earth Planet. Sci. Lett.*, *63*, 353–367.

Dunlop, D. J. (2002), Theory and application of the Day plot (M_{rs}/M_s versus H_{cr}/H_c): 1. Theoretical curves and tests using titanomagnetite data, *J. Geophys. Res.*, *107*(B3), 2056, doi:10.1029/2001JB000486.

Dunlop, D. J. (2003), Stepwise and continuous low-temperature demagnetization, *Geophys. Res. Lett.*, *30*(11), 1582, doi:10.1029/2003GL017268.

Dunlop, D. J., and G. Kletetschka (2001), Multidomain hematite: A source of planetary magnetic anomalies?, *Geophys. Res. Lett.*, *28*, 3345–3348.

Dunlop, D. J., and Ö. Özdemir (1997), *Rock Magnetism: Fundamentals and Frontiers*, 573 pp., Cambridge Univ. Press, New York.

Dunlop, D. J., and Ö. Özdemir (2001), Beyond Néel's theories: Thermal demagnetization of narrow-band partial thermoremanent magnetizations, *Phys. Earth Planet. Inter.*, *126*, 43–57.

Dunlop, D. J., and S. Xu (1994), Theory of partial thermoremanent magnetization in multidomain grains: 1. Repeated identical barriers to wall motion (single microcoercivity), *J. Geophys. Res.*, *99*, 9005–9023.

Dunlop D. J., S. Xu, and F. Heider (2004), Alternating-field demagnetization, single-domain-like memory, and the Lowrie-Fuller test of multidomain magnetite grains (0.6–356 μm), *J. Geophys. Res.*, *109*, B07102, doi:10.1029/2003JB003006.

Enkin, R. J., and W. Williams (1994), Three-dimensional micromagnetic analysis of stability in fine magnetic grains, *J. Geophys. Res.*, *99*, 611–618.

Fabian, K. (2000), Acquisition of thermoremanent magnetization in weak magnetic fields, *Earth Planet. Sci. Lett.*, *142*, 468–486.

Fabian, K. (2001), A theoretical treatment of paleointensity determination experiments on rocks containing pseudo-single or multi domain magnetic particles, *Earth Planet. Sci. Lett.*, *188*, 45–58.

Hill, M. J., and J. Shaw (2000), Magnetic field intensity study of the 1960 Kilauea lava flow, Hawaii, using the microwave palaeointensity technique, *Geophys. J. Int.*, *142*, 487–504.

Kono, M., and N. Ueno (1977), Paleointensity determination by a modified Thellier method, *Phys. Earth Planet. Inter.*, *13*, 305–314.

Kosterov, A. A., and M. Prévot (1998), Possible mechanisms causing failure of Thellier palaeointensity experiments in some basalts, *Geophys. J. Int.*, *134*, 554–572.

Levi, S. (1977), The effect of magnetite particle size on paleointensity determinations of the geomagnetic field, *Phys. Earth Planet. Inter.*, *13*, 245–259.

McClelland, E., A. R. Muxworthy, and R. M. Thomas (1996), Magnetic properties of the stable fraction of remanence in large multidomain (MD) magnetite grains: Single-domain or MD?, *Geophys. Res. Lett.*, *23*, 2831–2834.

Nagata, T., Y. Arai, and K. Momose (1963), Secular variation of the geomagnetic total force during the last 5000 years, *J. Geophys. Res.*, *68*, 5277–5281.

Néel, L. (1955), Some theoretical aspects of rock magnetism, *Adv. Phys.*, *4*, 191–243.

Newell, A. J., and R. T. Merrill (1999), Single-domain critical sizes for coercivity and remanence, *J. Geophys. Res.*, *104*, 617–628.

Riisager, P., and J. Riisager (2001), Detecting multidomain magnetic grains in Thellier palaeointensity experiments, *Phys. Earth Planet. Inter.*, *125*, 111–117.

Roquet, J., and E. Thellier (1946), Sur les lois numériques simples, relatives à l'aimantation thermorémanente du sesquioxyde de fer rhomboédrique, *C. R. Hebd. Seances Acad. Sci.*, *222*, 1288–1290.

Schmidt, V. A. (1973), A multidomain model of thermoremanence, *Earth Planet. Sci. Lett.*, *20*, 440–446.

Shcherbakov, V. P., and V. V. Shcherbakova (2001), On the suitability of the Thellier method of palaeointensity determinations on pseudo-single-domain and multidomain grains, *Geophys. J. Int.*, *146*, 20–30.

Shcherbakov, V. P., E. McClelland, and V. V. Shcherbakova (1993), A model of multidomain thermoremanent magnetization incorporating temperature-variable domain structure, *J. Geophys. Res.*, *98*, 6201–6216.

Shcherbakov, V. P., V. V. Shcherbakova, Y. K. Vinogradov, and F. Heider (2001), Thermal stability of pTRMs created from different magnetic states, *Phys. Earth Planet. Inter.*, *126*, 59–73.

Shcherbakova, V. V., V. P. Shcherbakov, and F. Heider (2000), Properties of partial thermoremanent magnetization in PSD and MD magnetite grains, *J. Geophys. Res.*, *105*, 767–782.

Thellier, E., and O. Thellier (1959), Sur l'intensité du champ magnétique terrestre dans le passé historique et géologique, *Ann. Géophys.*, *15*, 285–376.

Xu, S., and D. J. Dunlop (1993), Theory of alternating field demagnetization of multidomain grains and implications for the origin of pseudo-single-domain remanence, *J. Geophys. Res.*, *98*, 4183–4190.

Xu, S., and D. J. Dunlop (1994), Theory of partial thermoremanent magnetization in multidomain grains: 2. Effect of microcoercivity distribution and comparison with experiment, *J. Geophys. Res.*, *99*, 9025–9033.

Xu, S., and R. T. Merrill (1989), Microstress and microcoercivity in multidomain grains, *J. Geophys. Res.*, *94*, 10,627–10,636.

Yu, Y., and D. J. Dunlop (2003), On partial thermoremanent magnetization tail checks in Thellier paleointensity determination, *J. Geophys. Res.*, *108*(B11), 2523, doi:10.1029/2003JB002420.

D. J. Dunlop, Geophysics, Physics Department, University of Toronto, Toronto, Ontario, Canada M5S 1A7. (dunlop@physics.utoronto.ca)

S. Xu, JDL Digital Systems, 1033 Andover Park East, Seattle, WA 98188, USA. (derek@jdlds.com)